



# Image Sensor Communication via Light Trail Using Propeller LED Transmitter

Zhengqiang Tang , Graduate Student Member, IEEE, Jinxing Zheng , Graduate Student Member, IEEE, Takaya Yamazato , Senior Member, IEEE, and Shintaro Arai , Member, IEEE

**Abstract**—This article proposes an image sensor communication (ISC) system based on light trails using rotary LEDs. The light trail refers to an optical phenomenon where light appears elongated and forms a trajectory due to the movement of luminous objects. In this study, we developed a propeller LED transmitter (P-Tx) that rotates LEDs with a propeller to generate and transmit light trail signals. According to the LED's rotation radius, the proposed system segments light trails to achieve high-capacity data transmission at short distances and high-trust transmission at long distances. In addition, we perform the rotation coordinates system conversion for the captured light trails to accurately and simply detect the signal LEDs' coordinates. We experimentally evaluate the proposed system's communication performance and data rate. The experimental results demonstrate that our system is capable of meeting communication requirements at various distances and exhibits significant potential in enhancing the data transmission rate of ISC.

**Index Terms**—Image sensor communication, light trail, optical camera communication, propeller LED transmitter, rotation coordinates transform, visible light communication.

## I. INTRODUCTION

VISIBLE light communication (VLC) [1] is regarded as a kind of optical wireless communication [2], [3], [4] technique. As the name implies, VLC transfers information using light in the visible spectrum. The VLC technique has been used in a variety of fields, such as indoor wireless local area network [5], [6], underwater wireless communication [7], [8], [9], and intelligent transport systems [10], [11], [12], [13]. This technique simultaneously realizes various functions like lighting and visual displaying while sending data. In VLCs, light-emitting diodes (LEDs) and laser diodes are usually used as transmitting devices [14]. Sometimes displays are used as

VLC transmitters [15], [16], [17], [18], [19] as well. In this study, we focus on LED transmitters. According to [20], an LED could blink at a frequency exceeding 1 GHz. The optical signals are transmitted by modulating fast-blinking LEDs. There are usually two VLC-receiving devices: photodiodes and image sensors (cameras). Especially, VLC using an image sensor is called image sensor communication (ISC) [10], [11], [12], [13], [14] or optical camera communication (OCC) [21], [22].

The focus of our research is on ISC. In ISC systems, the receiver camera captures the blinking states of LEDs and outputs them as an image. Then, we detect and extract the LED pixel value to recover data. The main appeal of ISC is the ability to project the received lights onto the two-dimensional image sensor plane. Based on this feature, multiple LED lights could be received in a single image [23], and the signal and noise light sources can be spatially distinguished by image processing [24], [25], [26]. In addition, because ISC uses a camera as the receiver, the relative position between the transmitter and the receiver can be estimated using single-view geometry [27]. However, the data rate of ISC depends on the camera frame rate. Commercial cameras usually capture tens of frames per second. When we use commercial cameras as ISC receivers, they limit the amount of received data and bring latency to the data decoding because we cannot recover signals until the exposure of one frame is finished. Researchers are exploring several options to solve this problem. For receiving side, we can use image sensors with high time resolution such as high-speed cameras [28], or event cameras [29]. For the transmitting side, we can use an LED array to achieve parallel signal transmission [30]. Other methods like rolling shutter mechanism-based high-speed sampling [31], [32], multi-level luminance transmission using pulse wide modulation [33], and polygon mirror type ISC scheme [34] were used to increase the data rate for ISC as well.

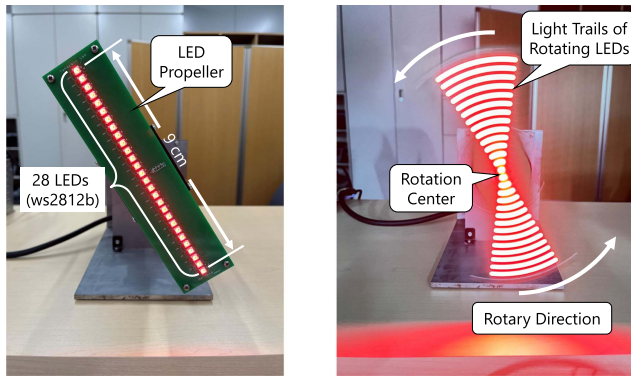
In previous studies, we developed a rotary LED transmitter [35], [36], [37] to improve the data rate for ISC. The transmitter has a rotary part in which several LEDs are arranged in a column. The rotary part is rotated with LEDs around a vertical axis. We switch the blinking states while rotating the LEDs to transmit optical signals. During the camera exposure time, 180 degrees of LED blinking states are recorded in the captured image as afterimages. In this case, a large number of LED blinks could be captured in a single image with a few LEDs, thus improving the data rate for ISC. In the previous study, the rotary LED transmitter rotates LEDs around a vertical axis to transfer data in all horizontal directions.

Manuscript received 29 June 2023; revised 3 September 2023; accepted 14 September 2023. Date of publication 19 September 2023; date of current version 3 October 2023. This work was supported in part by the Nagoya University and JST, the establishment of university Fellowships towards the creation of science technology innovation under Grant JPMJFS2120 for Nagoya University Interdisciplinary Frontier Fellowship, in part by JSPS KAKENHI under Grant JP21K11948, and in part by the Joint Research Program of the Institute of Materials and Systems for Sustainability, Nagoya University. (Corresponding author: Shintaro Arai.)

Zhengqiang Tang, Jinxing Zheng, and Takaya Yamazato are with the Nagoya University, Nagoya 464-8603, Japan (e-mail: tang@katayama.nuee.nagoya-u.ac.jp; jzheng@katayama.nuee.nagoya-u.ac.jp; yamazato@nagoya-u.jp).

Shintaro Arai is with the Okayama University of Science, Okayama 700-0005, Japan (e-mail: 0000-0002-4562-9385arai@ous.ac.jp).

Digital Object Identifier 10.1109/JPHOT.2023.3317082



(a) 28 LEDs arranged on the propeller. (b) Light trails during the rotation.

Fig. 1. Propeller LED transmitter (P-Tx). The P-Tx has several LEDs arranged in a line and rotates these LEDs with a propeller. During the camera's exposure time, the rotating LEDs' lights are stretched to generate light trails. Rotating the same angle, the outside LEDs' light trails are longer than the inside ones.

This article focuses on another rotation type and develops a propeller LED transmitter (P-Tx), as shown in Fig. 1. The P-Tx rotates LEDs in the shape of a propeller. We arrange several LEDs in a row on the propeller and rotate these LEDs with the propeller. We switch the LED blinking state according to the angle of rotation. The rotating LED lights generate light trails that are captured by the camera as afterimages. The camera shutter speed is set to be equal to the transmitter's rotation speed. We set the camera exposure time to the maximum value, meaning the camera read-out time could be neglected in this study. In this case, the proposed system can capture 360 degrees of LED lights, indicating we can further increase the data rate compared with the previous system [36]. Moreover, considering the proposed system's versatility, many applications use propeller-type rotation in the real world, such as propellers, windmills, and the persistence of vision displays [38]. Based on this fact, the proposed system is practical for general use because it can be easily integrated into these applications.

However, the spatial resolution of the signal LEDs varies during the rotation in the proposed system. For LEDs with different rotation radii, using a constant rotation angle to transmit the same bits of data, as in the previous study [36], could lead to issues of insufficient resolution or wastage of data transmission efficiency. This is because the linear velocity of the LED varies depending on its rotation radius. Regarding linear velocity, LEDs with large radii rotate faster than those with small radii. Rotating the same angle, the LEDs on the outside of the rotation take a longer path than the LEDs near the center of rotation. The increased light trail length implies that the outside LEDs have a more ample spatial resolution than the inside LEDs. To ensure that all LEDs have sufficient resolution on the image sensor, we first need to set a proper rotation angle that transmits 1 bit of data for the inside LEDs. With an increase in the rotation radius, if all the LEDs transmit the same bits of data using the same rotation angle, the signal light trails of the outside LEDs will be much longer than those of the inside LEDs. Sending the same number of bits of data with a long light trail as with a short trail is equivalent to sending data with a wasted length

of light trail. To improve the data transmission efficiency and satisfy communication requirements at different distances, we propose a zone-segment data transmission method for our new system. Specifically, we segment light trails into several zones depending on the rotation radii and optimize the length of the 1-bit signal light trail in different zones. With an increase in the rotation radius of each zone, we increase the transmitting signal density by decreasing the rotation angle that the LED transmits 1-bit data. This allows the increased amount of data that the outside LEDs transmit, thus improving the transmission efficiency of the proposed system. In addition, the proposed system can achieve ISC at different distances. The luminous density of rotating LEDs varies depending on the rotation radii. Light trails with small radii have high luminous density, thus having high luminance, which could transfer over long distances. Light trails with large radii have long trajectories, which could store large bits of data, and are appropriate for short-distance communication.

Furthermore, we propose a rotation coordinates transform method to simply and accurately detect the LED coordinates for our system. The receiver camera captures LEDs rotating with a propeller and outputs the light trails in circle shapes. To accurately measure the circle-shaped light trails, the receiver must precisely detect the rotation center and the radius of the LED. A slight deviation in the rotation center and radius calculation will reduce the accuracy of the LED coordinates detection. To solve this problem, we proposed a rotation-coordinates-transform signal detection method that conducts coordinates system transformation twice to convert the light trails captured in pixel coordinates into rotation coordinates. After the transform method, the light trails captured in circles are converted into line segments. In this case, the LED coordinates could be detected straightforwardly and accurately even in the presence of deviations in the center and radius calculation.

The novelties of the proposed system lie in the following points. First, we have developed the P-Tx that rotates LEDs in the shape of a propeller. In this case, more data could be received in one rotation compared with the previous study [36]. Second, depending on the rotation radius of the LED, we propose a zone-segment transmission method. This transmission method improves the data transmission efficiency for the proposed system and is expected to meet various communication requirements at different distances. Third, we propose a rotation coordinates transformation method to simplify the LED detecting process. The proposed transformation method converts LED light trails arranged in circles to one-dimension (1-D) line segments. In this case, the LED coordinates could be detected simply and accurately.

The remainder of this article is organized as follows. In Sect. II, the system model of the proposed ISC using the P-Tx is presented. In Sect. III, we analyze the characteristics of the light trail-based signal transmission from the perspective of luminous energy density and introduce the zone-segment data coding method. In Sect. IV, the decoding method based on the rotation coordinates system conversion is explained. In Sect. V, we experimentally evaluate the communication performance and

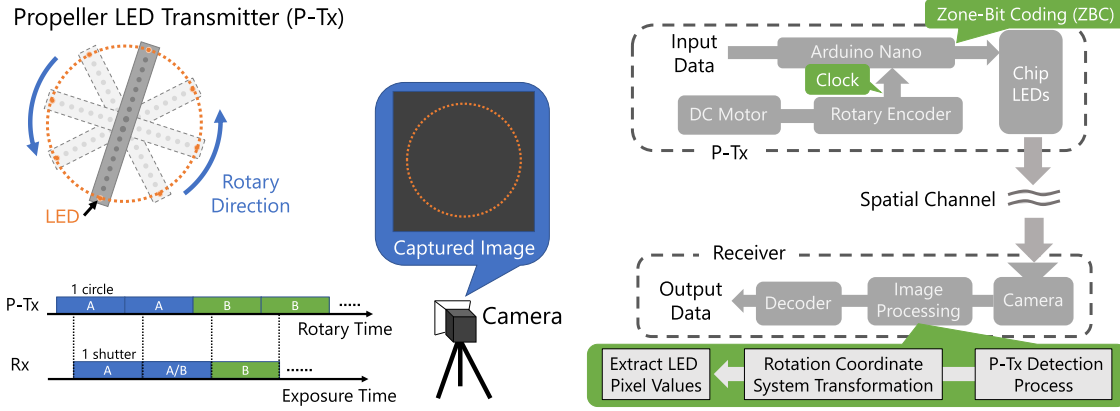


Fig. 2. System model of the ISC using P-Tx. The binary input data are modulated by a microcontroller (Arduino Nano) and are allocated to each LED. We rotate the propeller and switch the LED blinking states to transfer the optical signals. The camera's shutter speed and the P-Tx's rotary speed are set to be the same. We transmit the same symbol using two circles so the receiver can capture an entire symbol pattern on one frame in asynchronous communications.

the data rate of the proposed ISC system. Finally, a conclusion to this study is provided in Sect. VI.

## II. SYSTEM MODEL

Fig. 2 illustrates a block diagram of the proposed ISC system using P-Tx. The transmitter uses intelligent control LEDs (ws2812b), in which the control circuit and RGB chip are integrated, to transfer optical signals. Typically, multiple LEDs are mounted in series and can be controlled via just one data pin. Therefore, we can simplify the control circuit of multiple LEDs using this kind of ws2812b LEDs. We connect 14 LEDs in series and mount them equally spaced on one side of the propeller and mount 14 LEDs on the other side. LEDs on both sides of the propeller are central symmetry around the rotation center. We rotate the LED propeller with a DC motor through a timing belt. Besides the LED propeller, the rotating part has a microcontroller and a rotary encoder, as well as 8 AA batteries used to provide electricity. The rotary encoder generates a clock every one degree of rotation and simultaneously sends the clock to the microcontroller. The microcontroller modulates the binary data and allocates it to each LED once it receives the clock. We propose a zone-segment coding method that modulates data based on the LED rotation radius. The details of the coding methods are explained in Sect. III. According to the modulated data, the LED switches between ON and OFF to transfer binary signals.

LED lights carry transmitted signals and pass through the spatial channel. The camera captures the light trails and outputs them as an image. We set the shooting time of a frame equal to the time that the P-Tx rotates one circle. The P-Tx rotates one circle sending a symbol pattern. Here, let us consider a scenario in which P-Tx and the receiver operate asynchronously. P-Tx sends the same symbol pattern twice successively, as shown in Fig. 2. The receiver captures those patterns as two successive images. In this case, the receiver can completely capture one circle in one of the two captured images. Because the P-Tx circularly rotates LEDs, the camera captures LED lights arranged in circles. The image processing unit detects LED lights from the captured

image using the Hough gradient circle detection method [39]. Then, we measure the coordinates of LED lights by converting the pixel coordinates system into the rotation coordinates system. After the rotation coordinates transformation, LED lights are repositioned in 1-D for robust and easy detection. The luminance values of LEDs are then extracted and used to recover data.

## III. SIGNAL TRANSMISSION VIA LIGHT TRAIL

This section describes the signal transmission method based on the light trail, focusing on the ISC system using the P-Tx.

### A. Luminous Energy Density of a Rotating LED

During the signal transmission, LEDs move in a circular motion with the rotating propeller. The luminous energy density of a rotating LED varies because of the different rotation radii. The proposed system can simultaneously achieve short-distance, high-capacity, and long-distance, high-trust data transmission by leveraging the varying densities of luminous energy. In this section, we provide intuitive descriptions of the relationship between the luminous energy density and the rotation radius of an LED.

First, we consider a situation in which an LED without rotation continuously lights with constant power, as shown on the left side of Fig. 3. Let  $Q$  denote the luminous energy generated by the LED for the time  $t$ . The luminous energy is given by integrating luminous flux over a certain period of time as follows:

$$Q = \int_0^T \Phi(t) dt, \quad (1)$$

where  $\Phi$  indicates the luminous flux of an LED light source. With a fixed power supply, the luminous flux ( $\Phi$ ) of the same type of LED is considered constant. The luminous energy that the LED generates will increase when the lighting time increases. Therefore, we consider that the LED luminous energy ( $Q$ ) is proportional to the lighting time ( $t$ ), and (1) can be simplified as

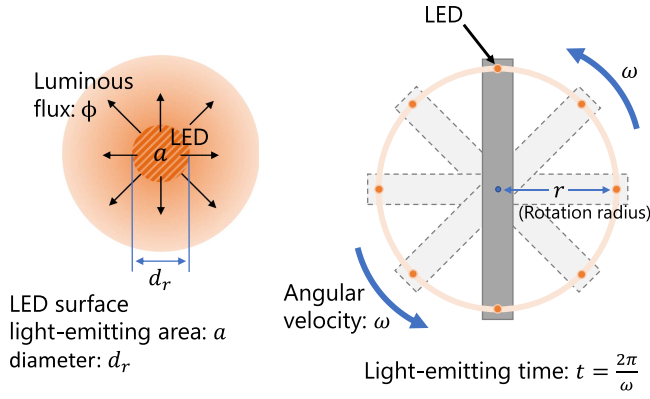


Fig. 3. Basic luminous energy analysis for a rotating LED. On the left side, a stationary LED is continuously lit with a constant power supply. The same LED with the same power supply rotates with a propeller is shown on the right side.

follows:

$$Q \propto t. \quad (2)$$

Let  $q$  denote the luminous energy density on the LED's light-emitting surface,  $q$  is given via multiplying  $Q$  by the reciprocal of the LED light-emitting area as follows:

$$q = Q \cdot a^{-1}, \quad (3)$$

where  $a$  indicates the light-emitting area of a stationary LED.

Now, we consider a case where an LED continuously lights and rotates with a propeller, as shown on the right side of Fig. 3. The time that the LED rotates for one circle is denoted by  $t_r$ , and  $t_r$  is calculated as follows:

$$t_r = \frac{2\pi}{\omega}, \quad (4)$$

where  $\omega$  is the angular velocity of the rotating LED. Let  $q_r$  and  $r$  denote the luminous energy density of the rotating LED and the rotation radius, respectively. Let  $d_r$  denote the diameter of the LED, as shown in Fig. 3. We calculate  $q_r$  as follows:

$$q_r = Q_r \cdot \frac{1}{2\pi r d_r}, \quad (5)$$

where  $Q_r$  is the luminous energy generated for time  $t_r$ . From (2), we know that  $Q_r$  is proportional to  $t_r$ . Therefore, (5) can be expressed as follows:

$$q_r \propto t_r \cdot \frac{1}{2\pi r d_r}. \quad (6)$$

Taking (4) into (6), we have the following relationship:

$$q_r \propto \frac{1}{\omega \cdot r \cdot d_r}. \quad (7)$$

If an LED is at the center of rotation, the rotation radius is 0, and the light-emitting area is  $a$ . The luminous energy density of the LED ( $q_0$ ) is expressed as follows:

$$q_0 \propto \frac{2\pi}{\omega} \cdot a^{-1} = \frac{2\pi}{\omega} \cdot \left( \pi \cdot \left( \frac{d_r}{2} \right)^2 \right)^{-1} = \frac{8}{\omega \cdot d_r^2}. \quad (8)$$

Combining (7) and (8), we can summarize the relationship between the luminous energy density and the linear velocity

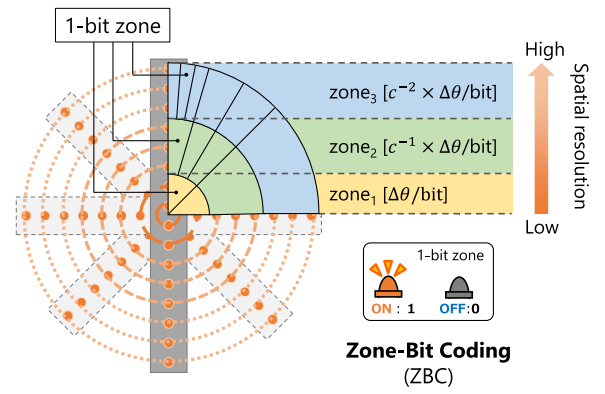


Fig. 4. Zone-bit coding for P-Tx. We segment the light trails into three zones based on the LED rotation radius. The different zones, progressing from the innermost to the outermost of the rotation, are referred to as zone<sub>1</sub>, zone<sub>2</sub>, and zone<sub>3</sub>, respectively.

of a rotating LED as follows:

$$q_r \propto \begin{cases} \frac{8}{\omega \cdot d_r^2}, & r = 0 \\ \frac{1}{\omega \cdot r \cdot d_r}, & r > 0 \end{cases}. \quad (9)$$

For a certain rotation speed of the P-Tx ( $\omega$ ) and a certain diameter of the LED ( $d_r$ ), the luminous energy density of the LED ( $q$ ) is inversely proportional to its rotational radius ( $r$ ). In short, when approaching the rotation center, the luminous energy density of the LED increases, resulting in high-brightness lights.

### B. Zone-Bit Coding Based on Rotation Radius

Here, we explain the proposed zone-segment coding method for the ISC using P-Tx. We call this coding method zone-bit coding (ZBC) in this study. The proposed ZBC is inspired by a computer storage technique called zone bit recording, which disk drives use to optimize the tracks for increased data capacity [40]. As shown in Fig. 4, we segment the light trails into three zones according to the rotation radii of LEDs. The zones from the inside to the outside are denoted by zone<sub>1</sub>, zone<sub>2</sub>, and zone<sub>3</sub>, respectively.

In zone<sub>1</sub>, we use the light trail generated by an LED rotating  $\Delta\theta$  [°] to transfer 1 bit of data. An LED's ON and OFF states in the corresponding 1-bit zone indicate the data '1' and '0,' respectively. For instance, if zone<sub>1</sub> contains 5 LEDs and the value of  $\Delta\theta$  is set to 45°, the throughput in zone<sub>1</sub> will be  $5 \times (360^\circ/45^\circ) = 40$  bits per rotation. With an increase in the rotation radius, the spatial resolution of P-Tx increases. The increased spatial resolution means more data bits could be transmitted during a rotation. To improve the data transmission efficiency, we multiply the rotation angle of the 1-bit light trails between adjacent zones by the inverse of a factor denoted by  $c$ . This study calls the factor  $c$  the zone resolution multiplier factor. Specifically, we use light trails of  $c^{-1} \times \Delta\theta$  [°] to transfer 1-bit data in zone<sub>2</sub> and  $c^{-2} \times \Delta\theta$  [°] to transmit 1-bit data in zone<sub>3</sub>. In summary, we rotate an LED for  $c^{-(k-1)} \times \Delta\theta$  [°] to transmit 1 b of data in zone<sub>k</sub>, where  $k$  is the index for a zone and  $k = 1, 2, 3$ . In this article, we segment light trails into three zones and set the zone resolution multiplier factor ( $c$ ) to 3 (i.e.,  $\Delta\theta$  in zone<sub>1</sub>,



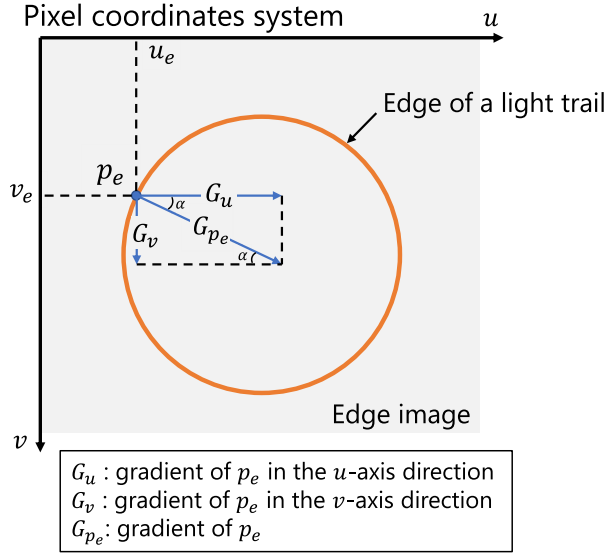


Fig. 5. Gradient of the point  $p_e$  at the edge of the circle-shaped light trail.

$3^{-1} \times \Delta\theta$  in zone<sub>2</sub>, and  $3^{-2} \times \Delta\theta$  in zone<sub>3</sub>). The number of segmented zones ( $k$ ) could be changed, and the value of  $c$  could also be varied between adjacent zones. The values of  $k$  and  $c$  should be optimized depending on the specific communication requirements. This article discusses the proposed system when  $k = 3$  and  $c = 3$ .

As analyzed in III-A, the luminous energy density of LED lights varies with different rotation radii. In zone<sub>1</sub>, light trails with high luminous energy density show a strong light intensity (i.e., high brightness). The high-brightness light trails could travel long distances and are less susceptible to interference from noise. Therefore, we use zone<sub>1</sub> for robust long-distance signal transmission. With increasing the rotation radius, the spatial resolution of P-Tx increases, and the number of bits that could be transmitted in a rotation also increases. The increased transmitting bits improve the capacity and efficiency of the data transmission for the proposed system. However, this improvement is achieved at the cost of attenuating luminous energy density. As the zone expands outward, the signal density increases, but the intensity of the light trails decreases accordingly. The low-brightness light trails are difficult to travel long distances. Therefore, we use light trails with long trajectories in zone<sub>3</sub> for short-distance high-capacity transmission.

#### IV. DETECTING AND DECODING PROCESS

The modulated light trail signals travel through the spatial channel and are captured by the receiver camera. This section describes the demodulation method for the light trail signal transmitted by the P-Tx.

##### A. The Detection Process for P-Tx

The receiver is required to locate the P-Tx from the captured image before data recovery. Because the P-Tx rotates LEDs with a propeller, the camera captures LED light trails in the shape of

circles. To detect the circle-shape light trails, we perform the Hough gradient circle detection method for the captured image.

Here, we introduce the principle of circle detection based on the Hough gradient method. We first perform the Canny method [41] for the captured image. The Canny method detects contours in the captured image and generates its edge image. Let  $I_e$  denote the matrix corresponding to the edge image. We measure the gradient direction for the edge image based on the Sobel convolution operation. Fig. 5 shows an edge image of a circle-shaped light trail in the pixel coordinate system. Let  $p_e$  denote a pixel at the circle-shaped light trail's edge. The horizontal and vertical pixel coordinates of  $p_e$  are denoted by  $u_e$  and  $v_e$ , respectively. The Sobel operator has two kernels, denoted by  $S_1(m, n)$ ,  $S_2(m, n)$ , are expressed as follows:

$$\begin{cases} S_1(m, n) = \begin{pmatrix} -1 & 0 & 1 \\ -2 & 0 & 2 \\ -1 & 0 & 1 \end{pmatrix} \\ S_2(m, n) = \begin{pmatrix} -1 & -2 & -1 \\ 0 & 0 & 0 \\ 1 & 2 & 1 \end{pmatrix} \end{cases}, \quad (10)$$

where  $m$  and  $n$  are the indexes for the elements of  $S$  as follows:

$$S(m, n) = \begin{pmatrix} s(-1, -1) & s(0, -1) & s(1, -1) \\ s(-1, 0) & s(0, 0) & s(1, 0) \\ s(-1, 1) & s(0, 1) & s(1, 1) \end{pmatrix}. \quad (11)$$

Let  $G_u$  and  $G_v$  denote the horizontal and vertical gradient values of  $p_e$ , respectively. The values of  $G_u$  and  $G_v$  are obtained by respectively convolving  $S_1$  and  $S_2$  with  $I_e$  as follows:

$$\begin{cases} G_u = \sum_{m=-1}^1 \sum_{n=-1}^1 S_1(m, n) \cdot I_e(u_e + m, v_e + n) \\ G_v = \sum_{m=-1}^1 \sum_{n=-1}^1 S_2(m, n) \cdot I_e(u_e + m, v_e + n) \end{cases}. \quad (12)$$

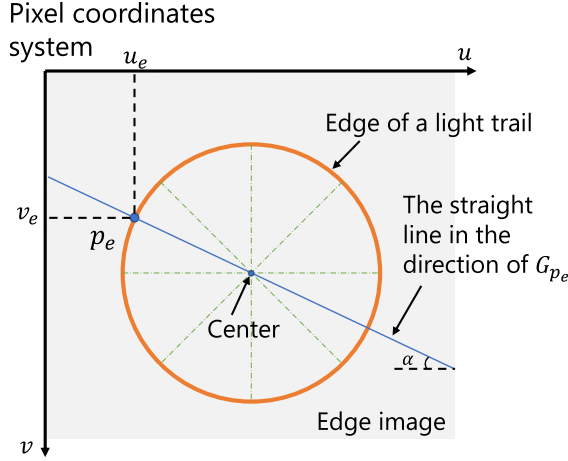
Let  $G_{p_e}$  denote the gradient of  $p_e$  and  $\alpha$  denote the direction of  $G_{p_e}$ , the value of  $\alpha$  is calculated as follows:

$$\alpha = \text{atan2}(G_v, G_u), \quad (13)$$

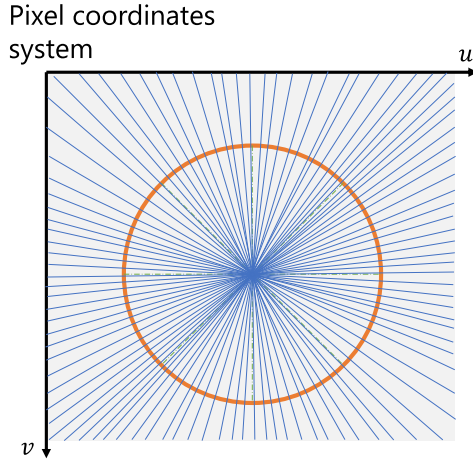
where  $\text{atan2}$  is denoted as follows:

$$\text{atan2}(j, i) = \begin{cases} \arctan\left(\frac{j}{i}\right), & \text{if } i > 0 \\ \arctan\left(\frac{j}{i}\right) + \pi, & \text{if } i < 0 \text{ and } j \geq 0 \\ \arctan\left(\frac{j}{i}\right) + 2\pi, & \text{if } i < 0 \text{ and } j < 0 \\ \frac{\pi}{2}, & \text{if } i = 0 \text{ and } j > 0 \\ \frac{3\pi}{2}, & \text{if } i = 0 \text{ and } j < 0 \\ 0, & \text{if } i = 0 \text{ and } j = 0 \end{cases}. \quad (14)$$

Then, we draw a straight line in the gradient direction ( $\alpha$ ) through the point  $p_e$  as shown in Fig. 6(a). Theoretically, this line will pass through the circle's center. Therefore, we vote for each pixel the line passes through. Next, we draw straight lines for each pixel point of the edge in the direction of the corresponding gradient and vote for each line. As shown in Fig. 6(b), the pixel near the circle's center is supposed to have the most votes. Based on this factor, we determine the pixel with the most votes as the center of the circle-shaped light trail. The estimated center is denoted by  $c$ , and the pixel coordinates of  $c$  are indicated by



(a) Draw a straight line through  $p_e$  in the gradient direction of  $G_{p_e}$ . Theoretically, this line should pass through the center of the circle. Then, we cast a vote for each pixel that the line intersects.



(b) Draw straight lines for each pixel at the light trail in the direction of the corresponding gradient. The center of the circle-shaped light trail should be near the pixel with the most votes.

Fig. 6. Detecting the rotation center of the light trail using the Hough gradient method.

$(u_c, v_c)$ . Finally, we measure the distance between the center and edge pixels to locate the light trail from the captured image.

Noteworthy, because the gradient values of the captured image's edge are discrete, the calculated gradient value ( $G_{p_e}$ ) could be 0 in practice, which negatively affects the gradient direction ( $\alpha$ ) calculation. A method generally used to calculate  $\alpha$  accurately is calculating the gradient of pixels in the eight neighborhoods of the target edge pixel ( $p_e$ ). Then, obtain the final gradient value of  $p_e$  by weighting the gradient values of the target  $p_e$  and its eight neighborhood pixels.

### B. Rotation Coordinates System Transformation

We measure the exact coordinates of each blinking LED after the light trail detection. However, to calculate the coordinates of

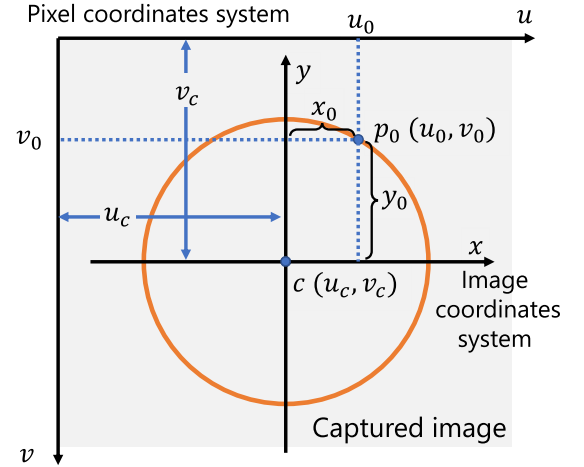


Fig. 7. Transform the pixel coordinates of the light trail into the image coordinates.

the LEDs on the circular light trail, the estimated center ( $c$ ) and the radius must be precise. Deviations in  $c$  or radius will affect the calculated LED coordinates, thus reducing the accuracy of the demodulation results. Here, we propose a simple and robust method to measure LED coordinates. This method transforms circular light trails in the pixel coordinates system into 1-D line segments in the rotation coordinates system.

First, let  $p$  denote a point on the light trail. The pixel coordinates of  $p$  is denoted by  $p_0(u_0, v_0)$  as shown in Fig. 7. First, we transform the light trail in the pixel coordinates into the image coordinates as follows:

$$\begin{cases} x_0 = u_0 - u_c \\ y_0 = v_c - v_0 \end{cases}, \quad (15)$$

where  $x_0$  and  $y_0$  are the transformed horizontal and vertical coordinates of  $p_0$  in the image coordinates system. We use the rotation center  $c$  estimated in Sect. IV-A as the origin of the image coordinates system.

Then, we transform the image coordinates system into the rotation coordinates system. Let  $p_i(x_0, y_0)$  denote the transformed image coordinates of the point  $p$ . We transform the image coordinates of  $p_i$  to rotation coordinates as follows:

$$\begin{cases} r_0 = \sqrt{x_0^2 + y_0^2} \\ \varphi_0 = \text{atan2}(y_0, x_0) \end{cases}. \quad (16)$$

Here,  $p_r(r_0, \varphi_0)$  denotes the coordinates of the point  $p$  in the rotation coordinates system. The definition of  $\text{atan2}$  can be referred to (14). As shown in Fig. 8, the light trail captured in the shape of a circle is transformed into a line segment after the rotation coordinates transformation. Because the light trail is arranged in 1 dimension in the rotation coordinates system, we can simply and accurately measure the coordinates of the blinking LEDs line by line. Then, we extract the LEDs' pixel values using the measured coordinates and recover data based on the threshold decision.

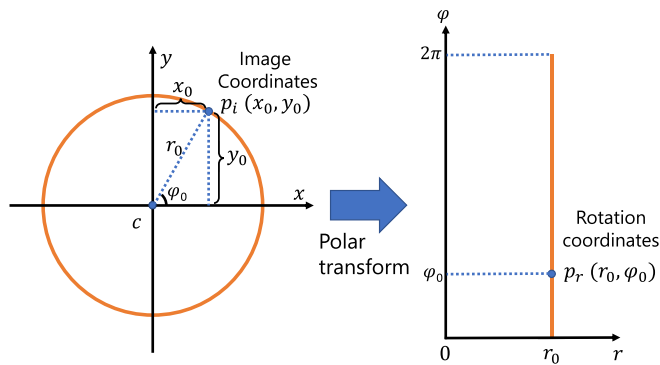


Fig. 8. Transform the image coordinates of the light trail into the rotation coordinates.

TABLE I  
EXPERIMENTAL SPECIFICATIONS

Experimental environment	Indoor
LED	ws2812b
Number of LEDs ( $N_L$ )	14
Number of zones ( $k$ )	3
Initial LED blinking angle ( $\Delta\theta$ )	45°
Zone resolution multiplier factor ( $c$ )	3
Rotary speed of P-Tx ( $S_r$ )	180 rpm
Camera	U3-3890SE-C-HQ
Image sensor resolution	3,000 × 4,000
Camera frame rate	3 fps
Exposure time	333,320 $\mu$ s
Focal length of Lens	35 mm
Aperture	F8
Lens filter	ND8
Communication distance	2.0–30.0 m

## V. PERFORMANCE EVALUATION

This study evaluates the communication performance of the proposed system through experiments. The experimental conditions are listed in Table I. The experiment was conducted in indoor environments, as shown in Fig. 9. We used 14 LEDs on one side of the propeller to transmit optical signals via light trails. We divided these light trails into three zones, and the number of LEDs used in each zone is allocated as follows: 4 LEDs in zone<sub>1</sub>, 5 LEDs in zone<sub>2</sub>, and 5 LEDs in zone<sub>3</sub>. The initial LED blinking angle in zone<sub>1</sub> ( $\Delta\theta$ ) was set to 45° and the zone resolution multiplier factor ( $c$ ) was set to 3. This means LEDs switch blinking states every 45°, 15°, and 5° in zone<sub>1</sub>, zone<sub>2</sub>, and zone<sub>3</sub>, respectively. The value of  $\Delta\theta$  and  $c$  could be optimized for different communication purposes. This study evaluated the proposed system using the above constant values. We rotated the P-Tx at a speed ( $S_r$ ) of 180 rotations per minute (rpm). A test scene that the P-Tx generates light trail signals based on ZBC is shown in Fig. 10.

The receiver camera used in this experiment is U3-3890SE-C-HQ (IDS Peak Family) with a 3,000 × 4,000 pixels image sensor. We set the camera frame rate to 3 frames per second

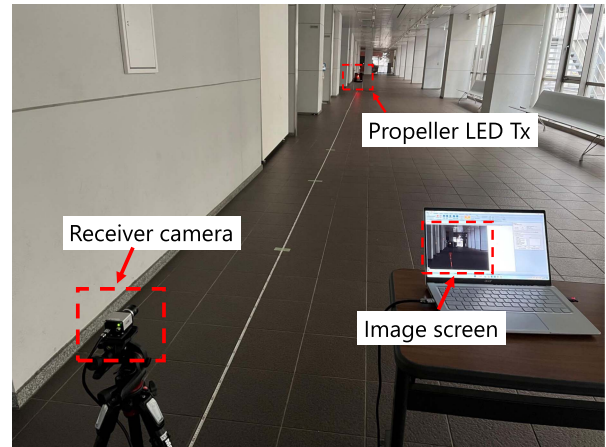


Fig. 9. Experimental setup. The experiments were conducted indoors on the ground floor of the IB Electronic Information Building, Nagoya University. We faced the P-Tx's light-emitting part to the receiver camera's lens and measured the demodulation performance from 2.0 m to 30.0 m.



Fig. 10. Test scene where P-Tx shows zone bit-coded light trails.

(fps) and the exposure time to 333,320  $\mu$ s. The camera used a lens with a focal length of 35 mm. We set the lens aperture to F8 and used an ND8 lens filter to prevent the saturation of the LED light received by the image sensor.

### A. Preliminary Operation Test

Before the communication performance evaluation, we performed a preliminary experiment to test the operation of our system. First, we send a test pattern to confirm the feasibility of the proposed ZBC and rotation coordinates system transformation methods. Specifically, we alternatively switched the LEDs' ON and OFF states for each zone and captured an image of the test pattern at 2.0 m. The captured test image is shown in Fig. 11. As the captured image in the pixel coordinates system shows, the camera successfully captured LEDs switching ON-OFF states every 45°, 15°, and 5° in zone<sub>1</sub>, zone<sub>2</sub>, and zone<sub>3</sub>, respectively. The transformed image in the rotation coordinates system is shown on the right side of Fig. 11. As one can see, the light trails captured in the circle shape are transformed into 1-D line segments. The coordinates of blinking LEDs can be easily measured in the transformed image. However, due to some

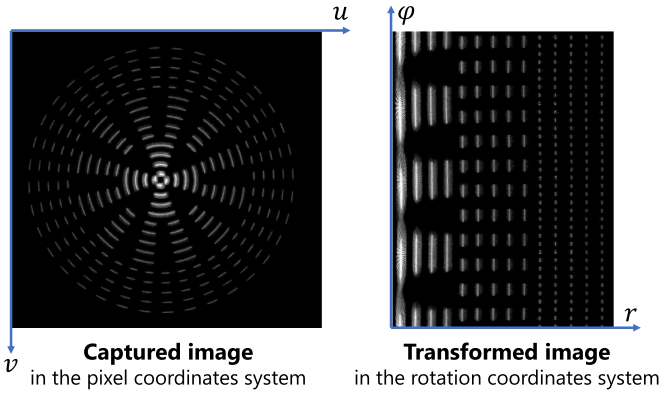


Fig. 11. Test image (trimmed) of the P-Tx using ZBC captured at 2.0 m and its transformed image in the rotation coordinates system.

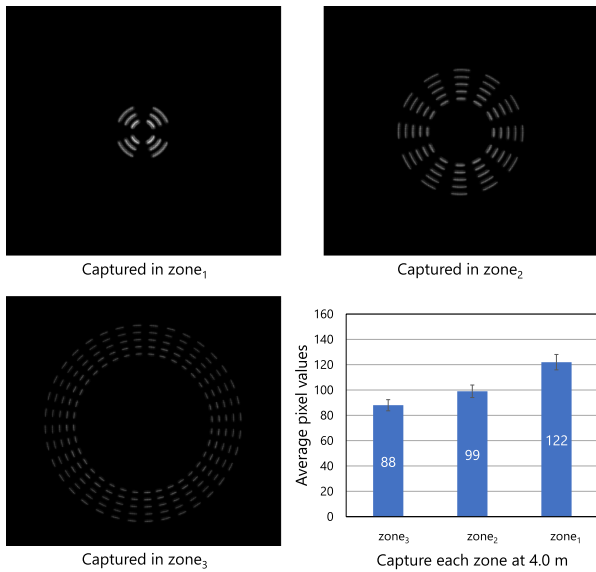


Fig. 12. Captured images (zoom in) of zone<sub>1</sub>, zone<sub>2</sub>, and zone<sub>3</sub> at 4.0 m.

hardware reasons, there is a noticeable blinking delay in the innermost LED. To avoid the impact of this LED (i.e., the LED with the smallest rotation radius), we set the innermost LED in the continuously ON state for detection purposes and performed communication experiments using the remaining 13 LEDs.

In addition, we captured images of zone<sub>1</sub>, zone<sub>2</sub>, and zone<sub>3</sub> separately to confirm our luminous energy density analysis of light trails described in Sect. III-A. As shown in Fig. 12, the brightness increases from zone<sub>3</sub> to zone<sub>2</sub>, and then to zone<sub>1</sub>. The average pixel values of light trails captured at 4.0 m in each zone are also shown in the same figure. From Fig. 12, we confirm the correctness of our luminous energy density analysis of rotating LEDs.

### B. Communication Performance Experiment

We experimentally evaluated the communication performance of our system after the operation test. The transmission sequence is shown in Fig. 13. As one can see, the transmission sequence consists of a pilot sequence and a data sequence. We

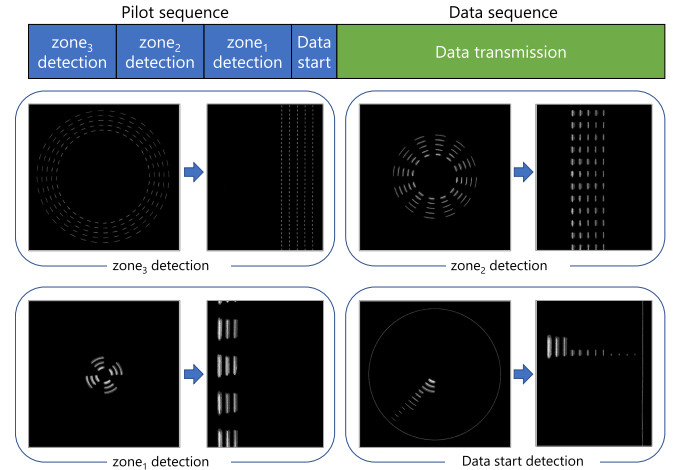


Fig. 13. Transmission sequence in the experiment.

used the pilot sequence to measure the LED coordinates for each zone and detect the data beginning. Specifically, we used three kinds of ON-OFF blinking patterns, which are the same as the captured images shown in Fig. 12, for coordinates detection of each zone. Then, we used one start pattern (see the bottom right of Fig. 13) to detect the beginning coordinates of the data transfer. The start pattern is also used to detect the location of the P-Tx from the captured image. In this experiment, we successfully measured LED coordinates using the Hough gradient method and the rotation coordinates transformation described in Sect. IV at short distances, indicating that these detecting methods are feasible. However, with increasing communication distance, the captured area of the P-Tx in the image decreases while the impact of background lights intensifies. Consequently, the accuracy of the Hough gradient detection method decreases. As an initial solution to this issue, we manually trimmed out the approximate region of P-Tx in the captured images at long distances and then performed the detecting process. This solution was only employed for the captured images in the pilot sequence, while the images captured in the data sequence were devoid of human intervention. The data transmission begins after the pilot sequence. We randomly generated and transmitted the data by blinking the zone-bit coded LEDs. In the decoding process, we assume that the receiver knows the position of the pilot sequence in the captured image sequence. During the experiment, the P-Tx and receiver camera positions were fixed. We recovered data using the threshold decision. The average pixel values of light trails for each zone at different distances were calculated as the threshold values. If the detected pixel value of the light trail signal is greater than or equal to the threshold value, we demodulate the data as “1.” Otherwise, we demodulate the data as “0.” During the experiment, we set the communication distance from 2.0 to 30.0 m and measured the number of error bits for each zone every 2.0 m. Let  $d_c$  denote the communication distance. The bit error rate (BER) of zone<sub>k</sub> at distance  $d_c$  is calculated as follows:

$$\text{BER}_k[d_c] = \frac{\text{err}_k[d_c]}{\text{bits}_k}, \quad (17)$$



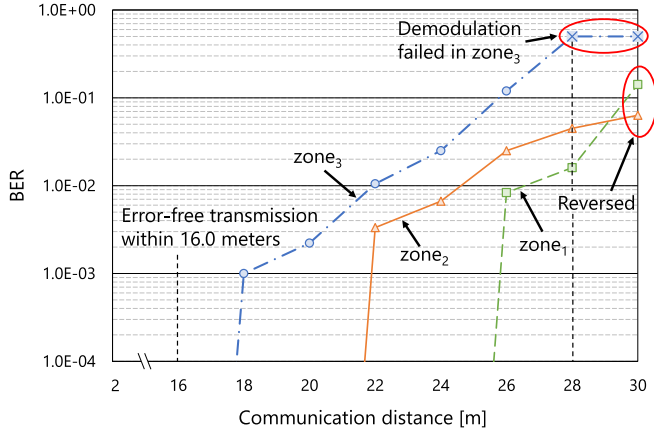


Fig. 14. Demodulation performance plotted in each zone against the communication distance.

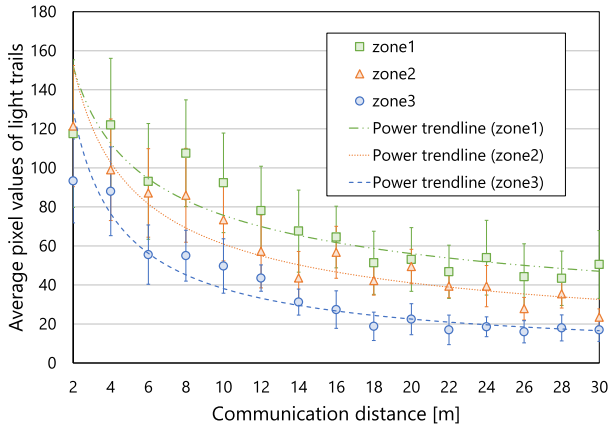


Fig. 15. Average pixel values of light trails plotted against the capture distance. The standard deviation on the value of the pixels obtained is shown as well.

where  $\text{err}_k[d_c]$  indicates the number of error bits in zone $_k$  at distance  $d_c$ , and  $\text{bits}_k$  indicates the number of transmitting bits in zone $_k$ .

Fig. 14 shows the BER versus communication distance. We measured the BERs of zone $_1$ , zone $_2$ , and zone $_3$  separately and plotted in the same graph. This experiment considers the BER less than  $10^{-3}$  error-free. As one can see, the error-free transmission distance of the proposed system is up to 16.0 m. The first demodulation errors occurred in zone $_1$ , zone $_2$ , and zone $_3$  were at 26.0 m, 22.0 m, and 18.0 m, respectively. This result reveals that each zone corresponds to different error-free transmission distances, which matches our prediction of the proposed ZBC in Sect. III-B. Therefore, we consider the proposed system applicable for data transmission at different distances. With an increase in communication distance, there is a gradual rise in the BER within each zone. The rise of BER is because of the variation of light intensity with distance and the spatial resolution of the image sensor.

Regarding the impact of the light intensity on the demodulation performance, we measured the average pixel values of light trails for each zone at different distances, as shown in Fig. 15. According to the inverse-square law [42], the light intensity is

inversely proportional to the square of the distance. Therefore, we applied power trendlines to approximate the relationship between received pixel values (brightness) and the communication distance. As shown in Fig. 15, the received average pixel values gradually decrease with increasing the communication distance. However, we found a huge difference between the measurement data and the power trendline at 2.0 m, especially for zone $_1$ . This phenomenon is mainly caused by the saturation of pixel values of the image sensor when capturing LED lights at close range. We calculated the average value using all pixels that light trails passed through. The pixel values around the center of the light trail are usually higher than those at the edges of the light trail. In this study, we used an 8-bit depth image sensor as the receiver. The maximum output pixel value of the image sensor is 255. When the received LED luminance exceeds the maximum value, the pixel value output from the image sensor remains 255. In close-range experiments, pixels around the center of the light trail are saturated. These saturated pixels reach the image sensor's maximum output value but are still lower than the actual luminance. As a result, the calculated average pixel value of the light trails at short distances is also lower than the actual luminance, thus resulting in a discrepancy between the measurement data and the power trendline. At the same distance, the pixel values of light trails sequentially increase from zone $_3$  to zone $_1$ . This result aligns with the luminous energy density analysis for the proposed system described in Sect. III-A. The luminous energy density of the light trails directly affects the received signal intensity (i.e., the received pixel values). Provided that the image sensor possesses ample resolution, the communication performance of the proposed system could be improved with an increase in the luminous energy density.

Now, we analyze the BER performance of our system for each zone in detail, starting with zone $_3$ . The BER of zone $_3$  gradually increases from  $1.0 \times 10^{-3}$  to  $1.2 \times 10^{-1}$  from 18.0 m to 26.0 m. This is mainly because the received light trails' brightness decreases with the increasing communication distance. At 28.0 m and 30.0 m, demodulation in zone $_3$  failed due to the unsuccessful coordinates detection. Fig. 16 shows coordinates detection images of zone $_3$  captured at 20.0 m and 28.0 m. We applied Otsu's method [43] to binarize the detection image, followed by measuring the center-of-gravity of these light trails as the coordinates of the LED signals. As one can see, LED light trails captured at 20.0 m were easy to distinguish and identify. However, when the communication distance increases to 28.0 m, the camera's lens is difficult to focus manually. The captured image could be blurred due to out-of-focus, leading to the image's brightness becoming flat. The flattened brightness has a negative impact on coordinates detection, especially in zone $_3$  with high signal density. As shown in Fig. 16, it is difficult to identify the light trails in the binarized detection image captured at 28.0 m, thus resulting in the signal coordinates detection and demodulation failures in zone $_3$ .

Then, we move our attention to zone $_2$ . As one can see, the BER trend of zone $_2$  is similar to that of zone $_3$ . Zone $_2$  outperformed zone $_3$  with respect to the demodulation performance because of its high luminous energy density ( $q_r$ ) and the long light trail.

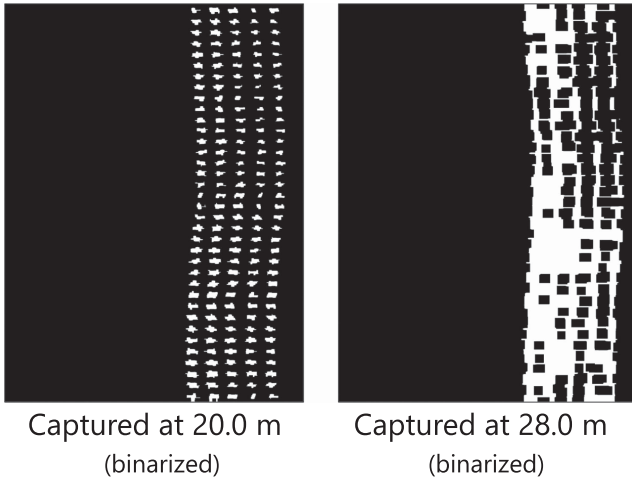
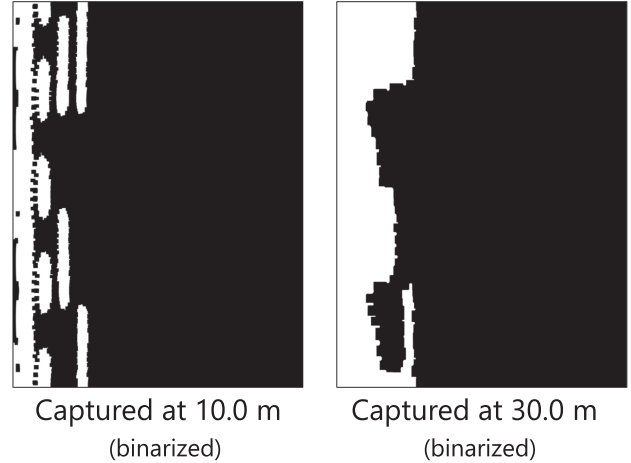
Coordinates detection images for zone<sub>3</sub>

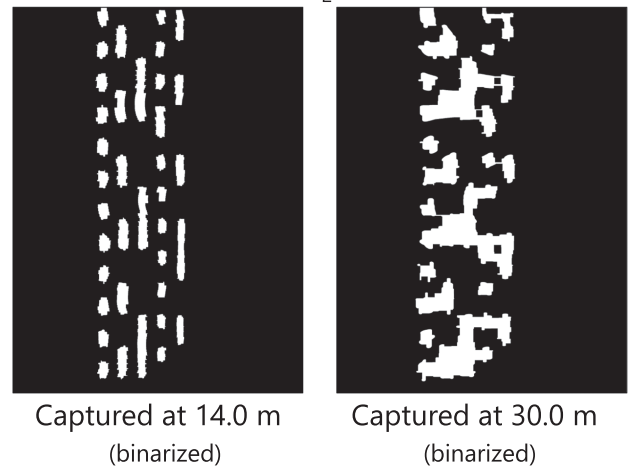
Fig. 16. Coordinates-detection-images (binarized) of zone<sub>3</sub> at 20.0 m and 28.0 m. The zone<sub>3</sub>'s coordinates detection fails at 28.0 m due to the out-of-focus.

Note that these two results are from the same experimental environment. Namely, the impact of the background noise on each zone at the same distance could be considered almost the same. With an increase in the luminous energy density of LED lights, the signal-noise ratio increases, thus improving the demodulation performance. In addition, when the LED is close to the center of rotation, we reduce the transmitting signal density (i.e., the number of transmitting bits) in the corresponding zone. This allowed the light trail transmitting a bit of data in zone<sub>2</sub> to be longer than that in zone<sub>3</sub>. The long light trails in zone<sub>2</sub> were easier to be identified compared with those in zone<sub>3</sub>, thereby further increasing the demodulation accuracy.

The zone<sub>1</sub> has the best BER performance in our system for its highest luminous energy density and longest light trail. However, we noted that the BER of zone<sub>1</sub> at 30.0 m is higher than that of zone<sub>2</sub>. This is because the spatial resolution of the image sensor is insufficient to distinguish the blinking states of the LED with a small rotation radius at 30.0 m. Fig. 17(a) shows the binarized data images of zone<sub>1</sub> in the rotation coordinates system at 10.0 m and 30.0 m. These two data images show the same transmitting signal pattern. The zone<sub>1</sub> consists of 4 LEDs where the innermost LED (i.e., the leftmost light trail) was constantly ON for detection purposes, and the remaining 3 LEDs are used for communications. As we can see, the signal pattern of zone<sub>1</sub> at 10.0 m could be recognized accurately. However, when the communication distance increases to 30.0 m, the blinking states become hard to identify, especially for the LEDs with small rotation radii. In this case, the OFF states of the LED's light trail failed to be recognized, thus negatively affecting the demodulation performance of zone<sub>1</sub>. On the other hand, the LEDs in zone<sub>2</sub>, characterized by larger rotation radii, did not face the same issue as those in zone<sub>1</sub> when positioned at a distance of 30.0 m. Fig. 17(b) shows the binarized data images of zone<sub>2</sub> with the same signal pattern at 14.0 m and 30.0 m. Here, the LED blinking states at 14.0 m indicate the correct

Demodulation for zone<sub>1</sub>

(a) The data-images of zone<sub>1</sub> in the rotation coordinates system at 10.0 m and 30.0 m. Due to the insufficient resolution issue, the blinking states of the LEDs with small rotation radii (i.e., the left light trails) are difficult to be distinguished at 30.0 m.

Demodulation for zone<sub>2</sub>

(b) The binarized data images of zone<sub>2</sub> with the same transmitting signal pattern at 14.0 m and 30.0 m. In particular, the data image at 14.0 m accurately represents the correct signal pattern. While LED lights interfered with each other in zone<sub>2</sub> at 30.0 m, most blinking states can be recognized more accurately compared to zone<sub>1</sub>.

Fig. 17. Examining why the BERs of zone<sub>1</sub> and zone<sub>2</sub> are reversed at 30.0 m.

signal pattern. Although LED lights in zone<sub>2</sub> also interfered with each other at 30.0 m, the majority of blinking states can still be identified with greater accuracy compared to zone<sub>1</sub>. This allows the BER of zone<sub>2</sub> outperformed that of zone<sub>1</sub> at 30.0 m. To quantitatively evaluate the communication performance of the proposed system, we fixed the focal length of the camera's lens and the resolution of the image sensor in this study. The BER performance could be further improved by using telephoto lenses [44] or using high-resolution image sensors [45].

Here, we explain the communication performance if all LEDs transfer signals using the same angular resolution. In this study,

TABLE II  
DATA RATE OF THE PROPOSED SYSTEM IN THE EXPERIMENT

	zone <sub>1</sub>	zone <sub>2</sub>	zone <sub>3</sub>	total
Number of signal LEDs	3	5	5	13
Data rate [bps]	72	360	1,080	1,512

we segmented light trails into zones and varied the rotation angle that transmits 1 bit of data in each zone. If we set the rotation angle that transmits 1-bit data to  $5^\circ$  for all LEDs as in zone<sub>3</sub> (i.e., modulate all LEDs without zone segment), the system's BER curve will converge to that of zone<sub>3</sub>, and its decoding accuracy could be lower than zone<sub>3</sub> when communicating over long distances for resolution reasons.

Finally, we evaluate the data rate of the proposed system. The data rates are different for each zone. Let  $R_{\text{zone}_k}$  [bps] denote the data rate in zone <sub>$k$</sub> , and  $R_{\text{zone}_k}$  is calculated as follows:

$$R_{\text{zone}_k} = N_{\text{zone}_k} \cdot \frac{360^\circ}{c^{-(k-1)} \times \Delta\theta} \cdot \frac{S_r}{60}, \quad (18)$$

where  $N_{\text{zone}_k}$  is the number of signal LEDs used in zone <sub>$k$</sub> . Specifically, we used 3 LEDs, 5 LEDs, and 5 LEDs to transmit signals in zone<sub>1</sub>, zone<sub>2</sub>, and zone<sub>3</sub>, respectively. Taking the experimental parameters listed in Table I, we calculate the  $R_{\text{zone}_k}$  as shown in Table II. As a result, the proposed system achieved a total data rate of 1,512 bps in this experiment. Although the rates of zones near the rotation center still need to be increased, the reliable transmission distance has been successfully extended by using ZBC. We achieved this rate using just 13 signal LEDs for transmitting binary signals, coupled with a camera operating at a frame rate of 3 fps. We can further improve the data transmission rate of our system by increasing the rotary speed ( $S_r$ ) of P-Tx or increasing the zone resolution multiplier factor ( $c$ ).

## VI. CONCLUSION

In this article, we proposed a light trail-based ISC system using P-Tx. The P-Tx rotates blinking LEDs with a propeller to generate light trails for signal transmission. The proposed method enhances the data transmission rate of ISC by using the light trail scheme to enlarge the receiving area of LED light on the image sensor. The expanded receiving area allows the receiver camera to capture a great number of blinks within an image, even with only a few transmitting LEDs. In addition, leveraging LEDs' varying luminous energy density characteristics at different rotational radii, we proposed a zone-bit transmission method for various communication distances. This method segments light trails into several zones based on the rotation radius, enabling short-distance, high-capacity, and long-distance, high-reliable signal transmission. Furthermore, in the receiving process, we transformed the captured light trails from the pixel coordinates into the rotation coordinates, leading the LED coordinates detection simple and accurate. Finally, we experimentally evaluated our system's communication performance and data rate. The experimental results revealed that the

proposed system is capable of achieving ISC at various distances and has good potential for improving the ISC data rate.

## VI. ACKNOWLEDGMENT

The authors would like to thank Prof. Masaaki Katayama (Nagoya Univ.), Prof. Toshiaki Fujii (Nagoya Univ.), Prof. Hironaka Okada (Nagoya Univ.), Prof. Tomohiro Yendo (Nagoya Univ. of Tech.), Prof. Koji Kamakura (Chiba Inst. of Tech.), and Prof. Masayuki Kinoshita (Chiba Inst. of Tech.) for useful discussions and suggestions.

## REFERENCES

- [1] T. Komine and M. Nakagawa, "Fundamental analysis for visible light communication system using LED lights," *IEEE Trans. Consum. Electron.*, vol. 50, no. 1, pp. 100–107, Feb. 2004.
- [2] H. Elgala, R. Mesleh, and H. Haas, "Indoor optical wireless communication: Potential and state-of-the-art," *IEEE Commun. Mag.*, vol. 49, no. 9, pp. 56–62, Sep. 2011.
- [3] S. Arai, M. Kinoshita, and T. Yamazato, "Optical wireless communication: A candidate 6G technology?," *IEICE Trans. Fundam.*, vol. E 104-A, no. 1, pp. 227–234, Jan. 2021.
- [4] Z. Wei, Z. Wang, J. Zhang, Q. Li, J. Zhang, and H. Y. Fu, "Evolution of optical wireless communication for B5G/6G," *Prog. Quantum Electron.*, vol. 83, pp. 1–27, May 2022.
- [5] H. Haas, L. Yin, Y. Wang, and C. Chen, "What is LiFi?," *J. Lightw. Technol.*, vol. 34, no. 6, pp. 1533–1544, Mar. 2016.
- [6] H. Haas, "LiFi is a paradigm-shifting 5G technology," *Rev. Phys.*, vol. 3, pp. 26–31, Nov. 2018.
- [7] H. Kaushal and G. Kaddoum, "Underwater optical wireless communication," *IEEE Access*, vol. 4, pp. 1518–1547, 2016.
- [8] Y. Ji, G. Wu, and C. Wang, "Generalized likelihood block detection for SPAD-based underwater VLC system," *IEEE Photon. J.*, vol. 12, no. 1, pp. 1–10, Feb. 2020.
- [9] M. F. Ali, D. N. K. Jayakody, and Y. Li, "Recent trends in underwater visible light communication (UVLC) systems," *IEEE Access*, vol. 10, pp. 22169–22225, 2022.
- [10] H. B. C. Wook, S. Haruyama, and M. Nakagawa, "Visible light communication with LED traffic lights using 2-dimensional image sensor," *IEICE Trans. Fundam.*, vol. E 89-A, no. 3, pp. 654–659, Mar. 2006.
- [11] T. Yamazato et al., "Image-sensor-based visible light communication for automotive applications," *IEEE Commun. Mag.*, vol. 52, no. 7, pp. 88–97, Jul. 2014.
- [12] T. Yamazato, "V2X communications with an image sensor," *J. Commun. Inf. Netw.*, vol. 2, no. 4, pp. 65–74, Dec. 2017.
- [13] M. Kinoshita et al., "Simplified vehicle vibration modeling for image sensor communication," *IEICE Trans. Fundam.*, vol. 101-A, no. 1, pp. 176–184, Jan. 2018.
- [14] Z. Tang and T. Yamazato, "Image sensor communication and its transmitting devices," *Opt. Commun.*, vol. 541, Aug. 2023, Art. no. 129545.
- [15] K. Liu, X. Wu, and X. Shu, "On display-camera synchronization for visible light communication," in *Proc. IEEE Vis. Commun. Image Process.*, 2015, pp. 1–4.
- [16] H. Okada, S. Sato, T. Wada, K. Kobayashi, and M. Katayama, "Preventing degradation of the quality of visual information in digital signage and image-sensor-based visible light communication systems," *IEEE Photon. J.*, vol. 10, no. 3, Jun. 2018, Art. no. 7903509.
- [17] R. Boubezari, H. Le Minh, Z. Ghassemlooy, and A. Bouridane, "Smartphone camera based visible light communication," *J. Light. Technol.*, vol. 34, no. 17, pp. 4121–4127, Sep. 2016.
- [18] A. Kawade, W. Chujo, and K. Kobayashi, "Smartphone screen to camera uplink communication with enhanced physical layer security by low-luminance space division multiplexing," in *Proc. IEEE VTS Asia Pacific Wireless Commun. Symp.*, 2022, pp. 176–180.
- [19] K. Shimei, K. Kobayashi, and W. Chujo, "A study on modulation and diversity methods based on uniform color space for digital signage and image sensor-based VLC," in *Proc. IEEE Int. Conf. Commun. Workshops*, 2022, pp. 1–6.
- [20] L. Wang et al., "1.3 GHz E-O bandwidth GaN-based micro-LED for multi-gigabit visible light communication," *Photon. Res.*, vol. 9, no. 5, pp. 792–802, May 2021.

- [21] P. Luo et al., "Experimental demonstration of RGB LED-Based optical camera communications," *IEEE Photon. J.*, vol. 7, no. 5, pp. 1–12, Oct. 2015.
- [22] *IEEE Standard for Local and Metropolitan Area Networks—Part 15.7: Short-Range Wireless Optical Communication Using Visible Light*, IEEE Std 802.15.7-2011, pp. 1–309, Sep. 6, 2011, doi: [10.1109/IEEESTD.2011.6016195](https://doi.org/10.1109/IEEESTD.2011.6016195).
- [23] K. Kamakura, "Image sensors meet LEDs," *IEICE Trans. Commun.*, vol. E 100-B, no. 6, pp. 917–925, Jun. 2017.
- [24] S. Arai, H. Matsushita, Y. Ohira, T. Yendo, D. He, and T. Yamazato, "Maximum likelihood decoding based on pseudo-captured image templates for image sensor communication," *Nonlinear Theory Appl., IEICE*, vol. 10, no. 2, pp. 173–189, Apr. 2019.
- [25] Y. Ohira, T. Yendo, S. Arai, and T. Yamazato, "High performance demodulation method with less complexity for image-sensor communication," *Opt. Exp.*, vol. 27, no. 15, pp. 21565–21578, Jul. 2019.
- [26] Z. Tang, S. Arai, T. Yendo, D. He, and T. Yamazato, "Sequential maximum likelihood decoding incorporating reliability determination for image sensor communication," *IEICE Commun. Exp.*, vol. 9, no. 8, pp. 365–370, Aug. 2020.
- [27] Z. Tang, D. He, S. Arai, and D. Zou, "Positioning-aided scheme for image sensor communication using single-view geometry," in *Proc. IEEE Int. Symp. Circuits Syst.*, 2019, pp. 1–5.
- [28] Y. Goto et al., "A new automotive VLC system using optical communication image sensor," *IEEE Photon. J.*, vol. 8, no. 3, Jun. 2016, Art. no. 6802716.
- [29] W. Shen, P. Chen, and H. Tsai, "Vehicular visible light communication with dynamic vision sensor: A preliminary study," in *Proc. IEEE Veh. Netw. Conf.*, 2018, pp. 1–8.
- [30] T. Nagura, T. Yamazato, M. Katayama, T. Yendo, T. Fujii, and H. Okada, "Tracking an LED array transmitter for visible light communications in the driving situation," in *Proc. IEEE 7th Int. Symp. Wireless Commun. Syst.*, 2010, pp. 765–769.
- [31] C. Danakis, M. Afgani, G. Povey, I. Underwood, and H. Haas, "Using a CMOS camera sensor for visible light communication," in *Proc. IEEE Globecom Workshops*, 2012, pp. 1244–1248.
- [32] C. W. Chow et al., "Display light panel and rolling shutter image sensor based optical camera communication (OCC) using frame-averaging background removal and neural network," *J. Light. Technol.*, vol. 39, no. 13, pp. 4360–4366, Jul. 2021.
- [33] R. Huang et al., "Simultaneous visible light communication and ranging using high-speed stereo cameras based on bicubic interpolation considering multi-level pulse-width modulation," *IEICE Trans. Fundam.*, vol. E106-A, no. 7, pp. 990–997, Jul. 2023.
- [34] Y. Imai, T. Ebihara, K. Mizutani, and N. Wakatsuki, "High-speed visible light communication using combination of low-speed image sensor and polygon mirror," *IEICE Trans. Fundam.*, vol. E99.A(1), no. 1, pp. 263–270, Jan. 2016.
- [35] S. Arai, Z. Tang, A. Nakayama, H. Takada, and T. Yendo, "Implementation experiment of a rotary LED transmitter for improving the transmission rate for image sensor communication," in *Proc. IEEE Globecom Workshops*, 2020, pp. 1–6.
- [36] S. Arai, Z. Tang, A. Nakayama, H. Takada, and T. Yendo, "Rotary LED transmitter for improving data transmission rate of image sensor communication," *IEEE Photon. J.*, vol. 13, no. 4, Aug. 2021, Art. no. 7300611.
- [37] Z. Tang, S. Arai, and T. Yamazato, "Simplified alamouti-type space-time coding for image sensor communication using rotary LED transmitter," *IEEE Photon. J.*, vol. 14, no. 1, Feb. 2022, Art. no. 7307007.
- [38] W. H. Al-Natshah, B. K. Hammad, and M. A. Abu Zaid, "Design and implementation of a cylindrical persistence of vision display," in *Proc. IEEE 6th Int. Conf. Elect. Electron. Eng.*, 2019, pp. 215–219.
- [39] J. Illingworth and J. Kittler, "The adaptive hough transform," *IEEE Trans. Pattern Anal. Mach. Intell.*, vol. PAMI-9, no. 5, pp. 690–698, Sep. 1987.
- [40] S. Chen and M. Thapar, "Zone-bit-recording-enhanced video data layout strategies," in *Proc. IEEE 4th Int. Workshop Model., Anal. Simul. Comput. Telecommun. Syst.*, 1996, pp. 29–35.
- [41] J. Canny, "A computational approach to edge detection," *IEEE Trans. Pattern Anal. Mach. Intell.*, vol. PAMI-8, no. 6, pp. 679–698, Nov. 1986.
- [42] N. Voudoukis and S. Oikonomidis, "Inverse square law for light and radiation: A unifying educational approach," *Eur. J. Eng. Technol. Res.*, vol. 2, no. 11, pp. 23–27, Nov. 2017.
- [43] N. Otsu, "A threshold selection method from gray-level histograms," *IEEE Trans. Syst. Man Cybern.: Syst.*, vol. 9, no. 1, pp. 62–66, Jan. 1979.
- [44] O. Dalgic, J. Singh, T. Farnham, and D. Puccinelli, "Augmenting a smartphone camera with a telephoto lens for enhanced LED-to-Camera communication," in *Proc. IEEE Wireless Commun. Netw. Conf.*, 2023, pp. 1–6.
- [45] I. Takayanagi and J. Nakamura, "High-resolution CMOS video image sensors," *Proc. IEEE*, vol. 101, no. 1, pp. 61–73, Jan. 2013.